NTATION PAGE

Form Approved
OMB NO. 0704-0188

1. AGENCY USE ONLY (Leave blank)	2. REPORT DATE	3. REPORT TYPE AND DATES COVERED
	November 10, 1992	Annual Tech. Report: 1 Oct 91 – 31 Sep 92

4. TITLE AND SUBTITLE

(U) High Resolution Measurements of Mixing and Reaction Processes in Turbulent Flows

5. FUNDING NUMBERS

PE – 61102F
PR – 2308
SA – BS
G – 89-0541
AFOSR

6. AUTHOR(S)

Werner J.A. Dahm

7. PERFORMING ORGANIZATION(S) AND ADDRESS(ES)

Gas Dynamics Laboratories
Department of Aerospace Engineering
The University of Michigan
Ann Arbor, MI 48109-2140

8. PERFORMING ORGANIZATION REPORT NUMBER

AFOSR-TR- 93 0029

9. SPONSORING ORGANIZATION NAME(S) AND ADDRESS(ES)

AFOSR/NA
Building 410
Bolling AFB, DC 20332-6448

10. SPONSORING ORGANIZATION REPORT NUMBER

11. SUPPLEMENTARY NOTES

12a. DISTRIBUTION / AVAILABILITY STATEMENT

Approved for public release; distribution is unlimited

12b. DISTRIBUTION CODE

ABSTRACT *(Maximum: 200 words)*

High resolution multi-dimensional imaging measurements were reported of the detailed structure of mixing and combustion processes in turbulent flows. These measurements are unique because they provide the first fully-resolved quantitative data on scalar dissipation rate field structure in turbulent reacting flows. These molecular mixing rate data were coupled with a two-parameter non-equilibrium reaction chemistry formulation to generate instantaneous maps of combustion species concentration and reaction rate fields in turbulent flames under varying degrees of chemical non-equilibrium. Results showed that the reaction zone structure transitioned smoothly from a thin layer-like structure to broad distributed reaction zones as the flame extinction limit was approached. Additionally, fully-resolved four-dimensional spatio-temporal imaging measurements were used to measure the larger scale topology of these scalar dissipation layers. Results showed that the distribution of layer separations is very nearly lognormal. This finding verified a recent analytical model of the multiplicative character of the repeated stretching and folding processes leading to this layer-like structure in the scalar dissipation fields in turbulent flows. This model, coupled with this two-parameter non-equilibrium reaction chemistry formulation, provides a simple approach for predicting the fine structure of molecular mixing and non-equilibrium reaction chemistry in turbulent combustion.

14. SUBJECT TERMS

Turbulent Flows; Turbulent Mixing; Turbulent Reacting Flows; Turbulent Combustion; Turbulent Flames

15. NUMBER OF PAGES

34

16. PRICE CODE

17. SECURITY CLASSIFICATION OF REPORT	18. SECURITY CLASSIFICATION OF THIS PAGE	19. SECURITY CLASSIFICATION OF ABSTRACT	20. LIMITATION OF ABSTRACT
Unclassified	Unclassified	Unclassified	UL

NSN 7540-01-280-5500

Standard Form 298 (890104 Draft)
Prescribed by ANSI Std. 239-18
298-01

Contents

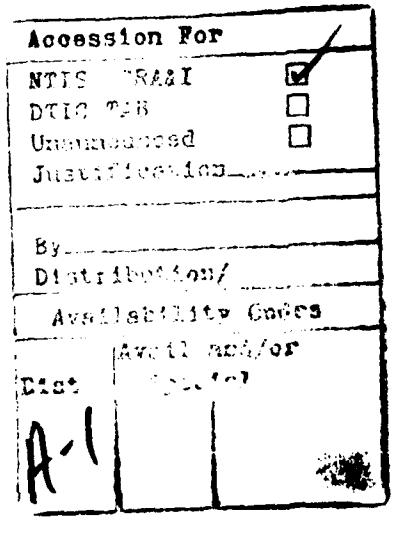

1. Summary of Research Progress

This section summarizes progress made during the reporting period in two major areas of the research. It begins with a brief introduction and overview of the research program in §1.1. Following this, §1.2 gives a summary of results from our study of the non-equilibrium structure of combustion in turbulent flows. Next, §1.3 summarizes results from measurements of the large scale topology and scaling properties of the scalar dissipation rate layers which form the basic feature of the molecular mixing process, and shows results from comparisons with an analytical model of the physical process that leads to this structure.

1.1 Introduction and Overview

This research program in the Gas Dynamics Laboratories at The University of Michigan consists of a combined experimental and theoretical investigation into the structure of combustion reactions in turbulent flows, with the following three major objectives:

(i) to develop and implement new, high-resolution, multi-dimensional, quantitative, imaging capabilities for obtaining direct experimental measurements of the fine scale structure associated with the molecular mixing and chemical reaction processes in turbulent flows,

(ii) to use these new measurement techniques to experimentally investigate the essential physical characteristics of the fine structure of molecular mixing and chemical reactions in turbulent flows, and

(iii) to incorporate results from these new experimental measurements into an improved understanding of the molecular mixing, chemical reaction, and local extinction processes in reacting turbulent flows of interest for practical air-breathing propulsion systems.

The overall goal of this program is to contribute to the development of new models for turbulent combustion in air-breathing propulsion systems. Such models are viewed as an essential tool in the development of future propulsion systems. Their development is, in turn, limited by the current lack of understanding of the nature of molecular mixing in turbulent flows and its

relation to complex combustion chemistry. This program is yielding important insights into the structure of reacting turbulent flows at the molecular diffusion and chemical reaction scales of the flow. It is based on direct measurements of the fully space- and time-varying fine structure of conserved scalar fields $\zeta(\mathbf{x},t)$ in nonreacting turbulent flows, and the relation between these and the physical structure of the corresponding chemical species concentration fields $Y_i(\mathbf{x},t)$ and the associated chemical reaction rate fields $w_i(\mathbf{x},t)$ in nonequilibrium reacting turbulent flows.

This Annual Report focuses on results obtained during the first year of this Phase II research effort. A number of basic concepts essential to the approach taken here, as well as results from our initial two-year start-up effort, are contained in the 1989-91 Final Report (see also AFOSR-TR-91-0111). Results have also been described in greater detail in several technical articles appearing in the refereed archival literature[1] as well as in several monograph articles and conference presentations[2].

Work in this program is proceeding along two major avenues. The first involves measurements conducted at moderate Reynolds numbers and large Schmidt numbers using a unique, four-dimensional, high-resolution, non-intrusive imaging capability developed under our Phase I effort. These four-dimensional imaging measurements are yielding fully-resolved, giga-byte sized, experimental data volumes of the precise conserved scalar field structure $\zeta(\mathbf{x},t)$

---

[1] see Dahm, Southerland & Buch (1991) *Physics of Fluids* A **3**, 1115-1127.
Tryggvason & Dahm (1990) *Combustion & Flame* 83, 207-220.
Chang, Dahm & Tryggvason (1991) *Physics of Fluids* A **3**, 1300-1311.
Southerland, Porter, Dahm & Buch (1991) *Physics of Fluids* A **3**, 1385-1392.
Dahm, Su & Southerland (1992) *Physics of Fluids* A **4**, 2191-2206.

[2] see Dahm, Southerland & Buch (1991) in Applications of Laser Techniques to Fluid Mechanics, R. Adrian, Ed., Springer Verlag, Berlin.
Dahm & Buch (1991) in Chemical Reactions and Physical Processes in Turbulent Flows, J. Hunt, Ed., Cambridge University Press.
Buch, Dahm, Dibble, & Barlow (1992) in Proceedings of the 24th International Symposium on Combustion, The Combustion Institute, Pittsburgh.
Dahm, W.J.A. (1992) in Proceedings of the 13th Symposium on Turbulence, University of Missouri-Rolla, Rolla, MO.
Dahm, W.J.A. (1992) in Turbulence and Molecular Processes in Combustion, T. Takeno, Ed., Elsevier.

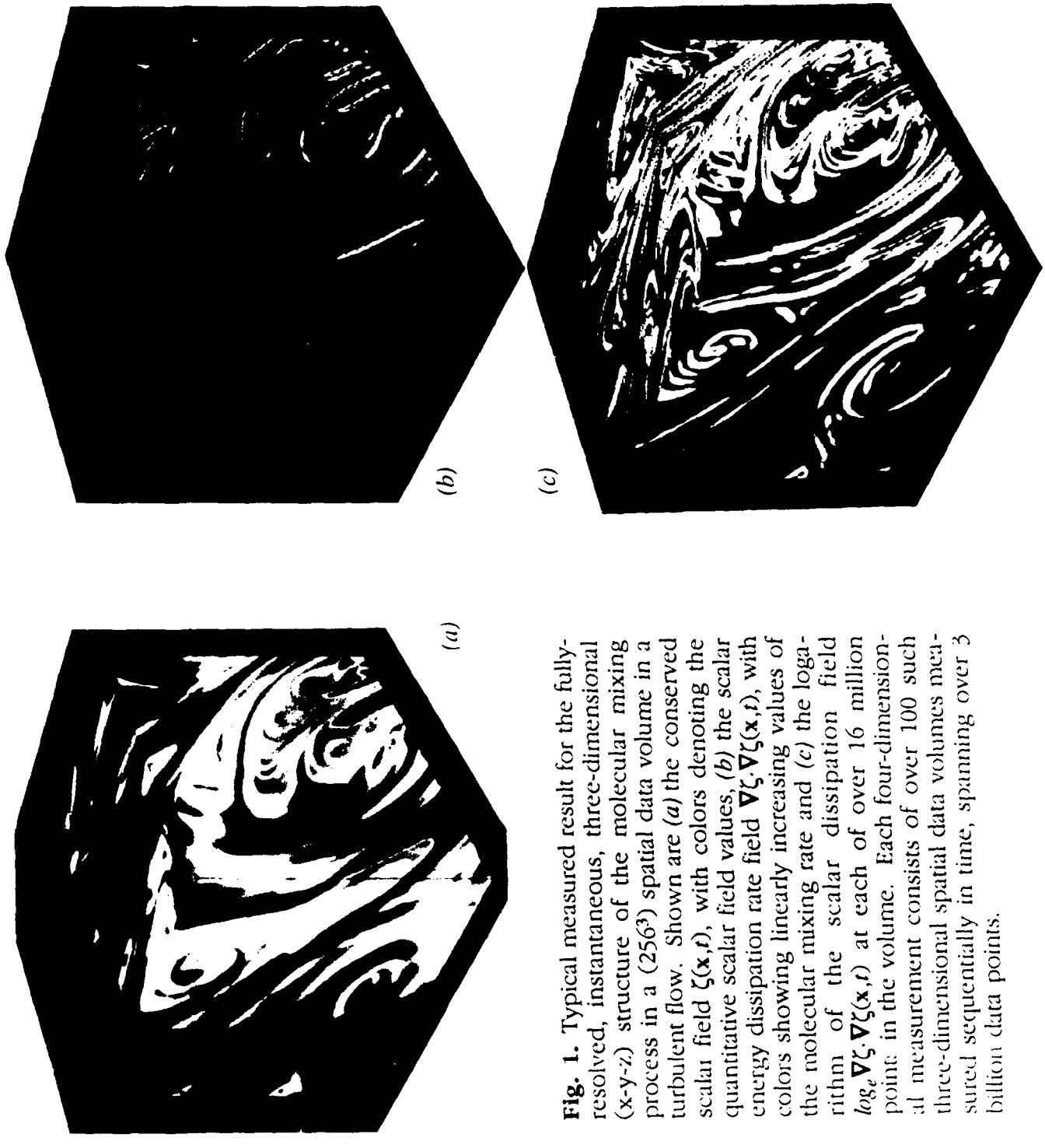

Fig. 1. Typical measured result for the fully-resolved, instantaneous, three-dimensional (x-y-z) structure of the molecular mixing process in a (256^3) spatial data volume in a turbulent flow. Shown are *(a)* the conserved scalar field $\zeta(\mathbf{x},t)$, with colors denoting the quantitative scalar field values, *(b)* the scalar energy dissipation rate field $\nabla\zeta\cdot\nabla\zeta(\mathbf{x},t)$, with colors showing linearly increasing values of the molecular mixing rate and *(c)* the logarithm of the scalar dissipation field $log_e\nabla\zeta\cdot\nabla\zeta(\mathbf{x},t)$ at each of over 16 million points in the volume. Each four-dimensional measurement consists of over 100 such three-dimensional spatial data volumes measured sequentially in time, spanning over 3 billion data points.

on the inner scales of turbulent flows (see Fig. 1). These data are simultaneously resolved in all three space dimensions and in time, allowing direct extraction of the instantaneous scalar energy dissipation rate field $\nabla\zeta\cdot\nabla\zeta(\mathbf{x},t)$ and its time evolution. These two fields can be used to deduce the mixing and chemical reaction processes in turbulent reacting flows. Data of this type have previously been conceivable only from large-scale direct numerical simulations (DNS) of the full Navier-Stokes equations, yet these experimental measurements are now possible in real turbulent flows and can reach conditions outside the range of accessibility of such numerical studies. Under our Phase I effort, these measurements were used to show that essentially all of the molecular mixing in turbulent flows occurs in thin, strained, laminar diffusion layers which can be accurately modeled by a simple canonical solution of the Navier-Stokes and conserved scalar transport equations. Under the present Phase II effort, the larger scale topology and scaling properties of these dissipation layers are being investigated to develop a complete model of the mixing process. These processes are driven by the continual stretching and folding imposed on the dissipation layers by the velocity gradient field in the underlying turbulent flow. Scaling properties deduced thus far show a remarkable similarity in the resulting dissipation field structure between high Reynolds number turbulent flows and simple low Reynolds number chaotic flows. This suggests great potential for the development of simple models of the molecular mixing process in practical turbulent flows.

Complementing these studies of molecular mixing in turbulent flows, a second major effort of our work involves highly-resolved, multi-dimensional imaging measurements of $Sc \approx 1$ conserved scalar mixing in gaseous turbulent flows. As is the case in our large Sc measurements, the highly resolved nature of the measurements, together with the very high signal quality achieved, permits direct differentiation of the data to allow accurate evaluation of derivatives involved in the scalar gradient field $\nabla\zeta(\mathbf{x},t)$. This yields the structure of scalar energy dissipation rate field, permitting highly detailed analysis of the structure of chemical reactions in nonequilibrium combustion processes occurring in turbulent flows. The local instantaneous thermochemical state of the reacting turbulent flow can be specified from a two-parameter nonequilibrium formulation in terms of the local conserved scalar and scalar dissipation rate values. This procedure is used to examine the reaction zone structure in

turbulent flames under varying degrees of chemical nonequilibrium. These measurements are providing a previously inaccessible level of detailed information about the structure of combustion processes in turbulent flows. Results obtained permit the first direct view into the structure of the species chemical reaction rate fields $w_i(\mathbf{x},t)$ in reactive turbulent flows under various degrees of chemical nonequilibrium.

1.2. Non-Equilibrium Structure of Turbulent Combustion

Experimental studies to identify the canonical structure of the instantaneous chemical reaction rate fields $w_i(\mathbf{x},t)$ in turbulent diffusion flames play a key role in the development of physically-based models of combustion in turbulent flames. Combustion models for turbulent reacting flow ultimately aim to represent the connection between the chemical source terms on the right side of the species conservation equations and the turbulent dynamics of the underlying flow field. Studies of the reaction zone structure under various conditions of turbulent flow are typically centered around single-point or planar imaging measurements of certain species concentration fields $Y_i(\mathbf{x},t)$, from which the reaction rate field structure is inferred. Instantaneous concentrations of such species as OH or CH, for example, have often been interpreted as approximately marking the reaction rate field structure. These concentration fields, however, reflect the cumulative effects of turbulent transport, molecular diffusion, and chemical reaction, and thus can give a potentially misleading picture of the underlying chemical reaction rate field structure

Direct measurements of the reaction rate fields are not possible, but they can be deduced from instantaneous measurements of a conserved scalar field $\zeta(\mathbf{x},t)$. In the limit of chemical equilibrium, for example, the structure of individual species reaction rate fields, $w_i(\mathbf{x},t)$, are relatively simply related (Bilger 1976) to the instantaneous conserved scalar value and the instantaneous dissipation rate, $(ReSc)^{-1}\nabla\zeta\cdot\nabla\zeta(\mathbf{x},t)$, of the scalar energy per unit mass, $^1/_2\zeta^2(\mathbf{x},t)$. Away from equilibrium, the connection between the scalar field structure and the reaction rate fields is not as simple. One approach to this is to use a strained laminar diffusion and reaction layer formulation to represent the interaction between the turbulent flow dynamics and the nonequilibrium reaction chemistry.

We are using this approach to examine the structure of instantaneous species mass fraction fields and the associated instantaneous chemical reaction rate fields in a turbulent jet diffusion flame under varying degrees of nonequilibrium chemistry. The objectives are, firstly, to assess the underlying canonical structure of nonequilibrium reaction rate fields in turbulent diffusion flames and, secondly, to determine the extent to which certain species concentration imaging measurements can be used as indirect indicators of the reaction field structure. The present results are for OH and NO mass fraction and reaction rate fields for hydrogen-air chemistry. The $Y_i(\mathbf{x},t)$ and $w_i(\mathbf{x},t)$ fields are constructed from fully-resolved imaging measurements of the instantaneous conserved scalar field $\zeta(\mathbf{x},t)$, obtained via planar Rayleigh scattering from the self-similar far field of a nonreacting turbulent jet flow.

Details of the flow facility, operating conditions, and imaging diagnostics are described elsewhere[4]. For the present purposes, the key points are that, at the flow conditions selected and for the imaging set-up used, the signal-to-rms-noise ratio that exceeded 100:1, and the smallest conserved scalar gradient scales were fully resolved in both space and time, reaching below the finest local scalar gradient lengthscale λ_D in the turbulent scalar field. This, together with the signal quality achieved, allows differentiation of the measured scalar field $\zeta(\mathbf{x},t)$ to produce the scalar dissipation rate field $\nabla\zeta\cdot\nabla\zeta(\mathbf{x},t)$. The self-similar far-field scaling of this flow allows these scalar and dissipation rate data to be mapped to any downstream location. The data are then coupled with a strained laminar flamelet library for hydrogen-air chemistry to produce the instantaneous species concentration and reaction rate fields for several increasing levels of chemical nonequilibrium. The Reynolds number is held constant while the Damköhler number is systematically varied by changing the effective nozzle diameter. Comparisons at different downstream locations in the jet allow effects due to the decreasing scalar values to be separated from effects due to the varying degree of nonequilibrium chemistry. We apply this approach to examine the OH and NO mass fraction and reaction rate fields under conditions reaching to deep nonequilibrium.

[4] see: Buch, Dahm, Dibble & Barlow (1991) Structure of equilibrium reaction rate fields in turbulent jet diffusion flames. *Proceedings of the 24th (International) Symposium on Combustion*, Sydney, Australia, July 5-10, 1992. See also Buch & Dahm (1991) Fine scale structure of conserved scalar mixing in turbulent shear flows. Sc » 1, Sc ≈ 1, and implications for reacting flows. *University of Michigan Report No. 026779-5.*

In our previous year report we showed a typical 256 × 512 measured data plane of the instantaneous conserved scalar field structure $\zeta(\mathbf{x},t)$. The 256 different colors denoted ranges of conserved scalar values, with pure blue beginning at $\zeta(\mathbf{x},t) = 0$, corresponding to pure air, and increasing uniformly to pure red denoting the highest conserved scalar values in the data. The jet centerline ran down the right edge of the data plane, and the axes indicated the spatial extent of the data in terms of the local strain-limited scalar gradient lengthscale λ_D. Derivatives of the measured conserved scalar field values give the projection of the true three-dimensional scalar gradient vector $\nabla\zeta(\mathbf{x},t)$ into the plane. We showed the logarithm of the corresponding scalar dissipation rate field formed from this projection, $log_e \nabla\zeta\cdot\nabla\zeta(\mathbf{x},t)$. The 256 different colors denoted the local scalar dissipation rate, with black beginning at $\nabla\zeta\cdot\nabla\zeta = 0$, and pure blue through pure red denoted logarithmically increasing values as indicated. These figures should be referred to in the following discussion. While two-dimensional dissipation values underestimate the magnitude of the full dissipation rate wherever the scalar gradient vector has a strong out-of-plane component, the present values nevertheless provide an accurate picture of the topological structure of the dissipation field.

The local outer variables $u(x)$ and $\delta(x)$, and the mass fraction-based conserved scalar field $\zeta(\mathbf{x},t)$, in the far field of axisymmetric turbulent jets follow known self-similar scalings with downstream location x. This allows measurements such as ours to be uniformly rescaled to map the instantaneous scalar and dissipation rate fields to any x-location in the far field of the flow. A set of hypothetical chemical reactions occurring in this conserved scalar field would then produce a turbulent jet diffusion flame of length L, where the flame tip is taken to occur at the x-location for which the maximum conserved scalar value achieves stoichiometry for the fuel and oxidizer combination being considered. The mass fraction and reaction rate fields for any chemical species *i* in this flame can then be constructed from the local values of the scalar and dissipation rate fields using a steady flamelet approximation.

Here we use a flamelet library for pure hydrogen-air strained laminar diffusion and reaction layers, generated from numerical calculations (supplied by J.-Y. Chen) using a subset of the Miller & Bowman (1989) hydrogen-air kinetic mechanism. Constructing the library requires mapping each (ζ, $\nabla\zeta\cdot\nabla\zeta$) pair to

the corresponding strain rate ε. The mapping obtained from the numerical calculations is shown in Fig. 2a. For small values of ζ, the calculations produce a nonunique mapping, presumably due to a nonuniqueness in defining the conserved scalar that results from differential species diffusivities. [For the highest strain rate ($\varepsilon \approx 14{,}000\ s^{-1}$), the map was also nonunique over the entire range of scalar values.] For this reason, the mapping was instead based on the analytical result for a nonreacting layer, given by

$$\varepsilon = \pi D \left[\frac{\nabla\zeta \cdot \nabla\zeta}{(\zeta^+ - \zeta^-)^2} \right] exp\, 2 \left\{ erf^{-1} \left[\frac{\zeta - \frac{1}{2}(\zeta^+ + \zeta^-)}{\frac{1}{2}(\zeta^+ - \zeta^-)} \right] \right\}^2 \cdot f(\zeta) \quad ,$$

where $f(\zeta)$ is chosen to fit the numerical result, accounting for effects of heat release and temperature dependent transport properties. This yields the mapping shown in Fig. 2b.

Here ζ^+ and ζ^- represent the scalar endpoint values on either side of the layer. For a layer separating pure fuel and air, as in the present library, these values are 0 and 1. However, as Fig. 1 demonstrates, none of the layers in the jet far field are bounded by pure fuel and air, and instead generally involve various degrees of partial premixing on one or both sides of the layer. A detailed treatment could take this into account but, as is generally done in flamelet models, in the present study any effect of varying endpoint values is ignored.

The OH mass fraction library $Y_{OH}(\zeta, \varepsilon)$ is shown in Fig. 3a, and the reaction rate library $w_{OH}(\zeta, \varepsilon)$ in Fig. 3b. A similar library is constructed for NO. For strain rates above $\varepsilon = 14{,}000\ s^{-1}$, the layer extinguishes and the flamelet library for $w_i(\zeta, \varepsilon)$ in Fig. 3b appropriately contains zero values. The mass fraction library in Fig. 3a also contains zero-OH concentrations in this domain of $Y_i(\zeta, \varepsilon)$, but these values are spurious since they correspond only to the steady state attained long after extinction. The species concentrations in the transient layer after extinction follow an exponential decrease due to the continued straining action of the flow field. A steady flamelet formulation cannot account for this transient (as well as other effects of unsteadiness), and therefore the zero OH and NO concentrations resulting from extinction in the $Y_i(\mathbf{x},t)$ fields presented in the following section only denote where extinction has occurred. The results obtained for the $w_i(\mathbf{x},t)$ fields, however, do not suffer this shortcoming, since

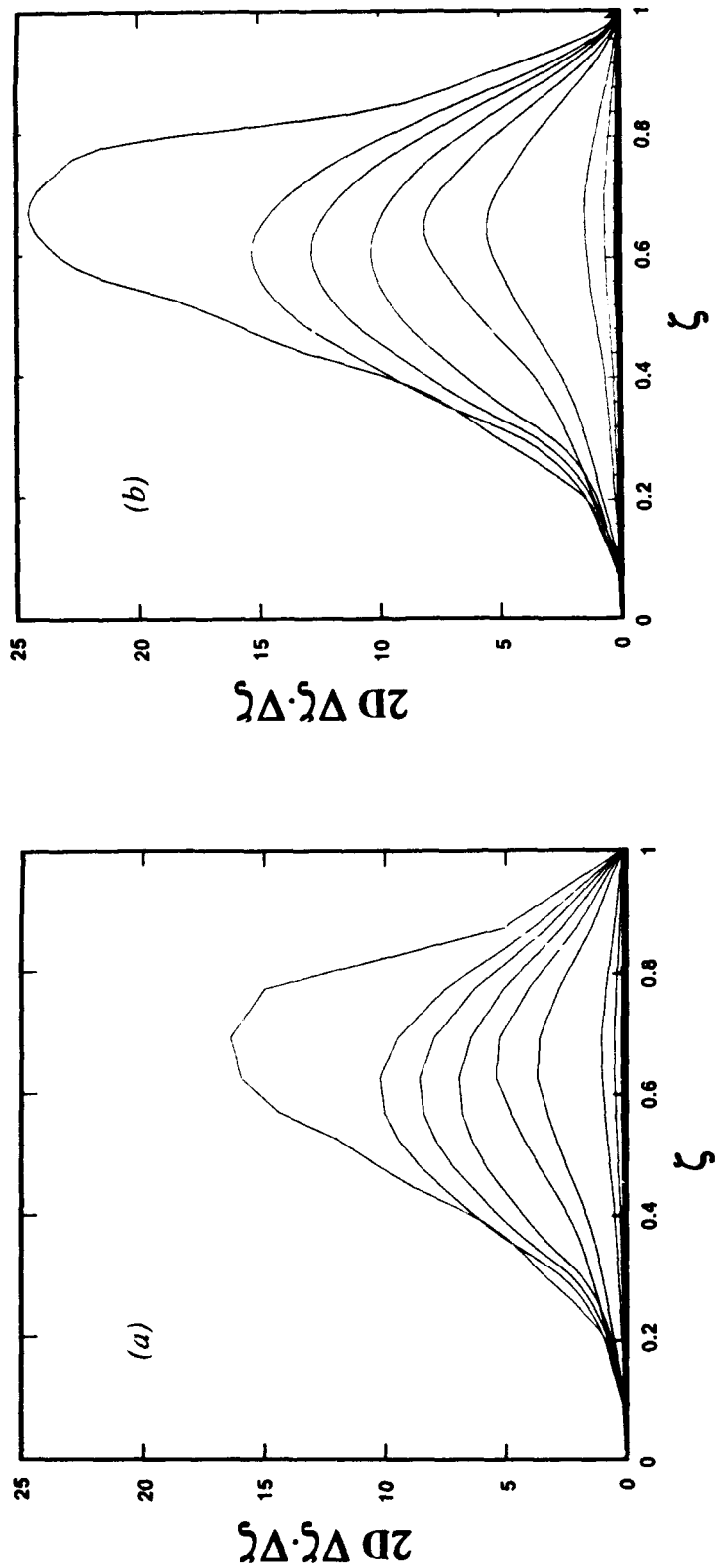

Fig. 2. Mapping from (ζ, $\nabla\zeta\cdot\nabla\zeta$) to the strain rate ε, from numerical calculations for hydrogen-air chemistry in an isolated strained laminar diffusion and reaction layer. Shown are contours for strain rates given by ε = 100, 400, 1000, 4000, 6000, 8000, 10 000, 12 000, and 14 000 s^{-1}. *(a)* Numerical result. *(b)* Analytical fit.

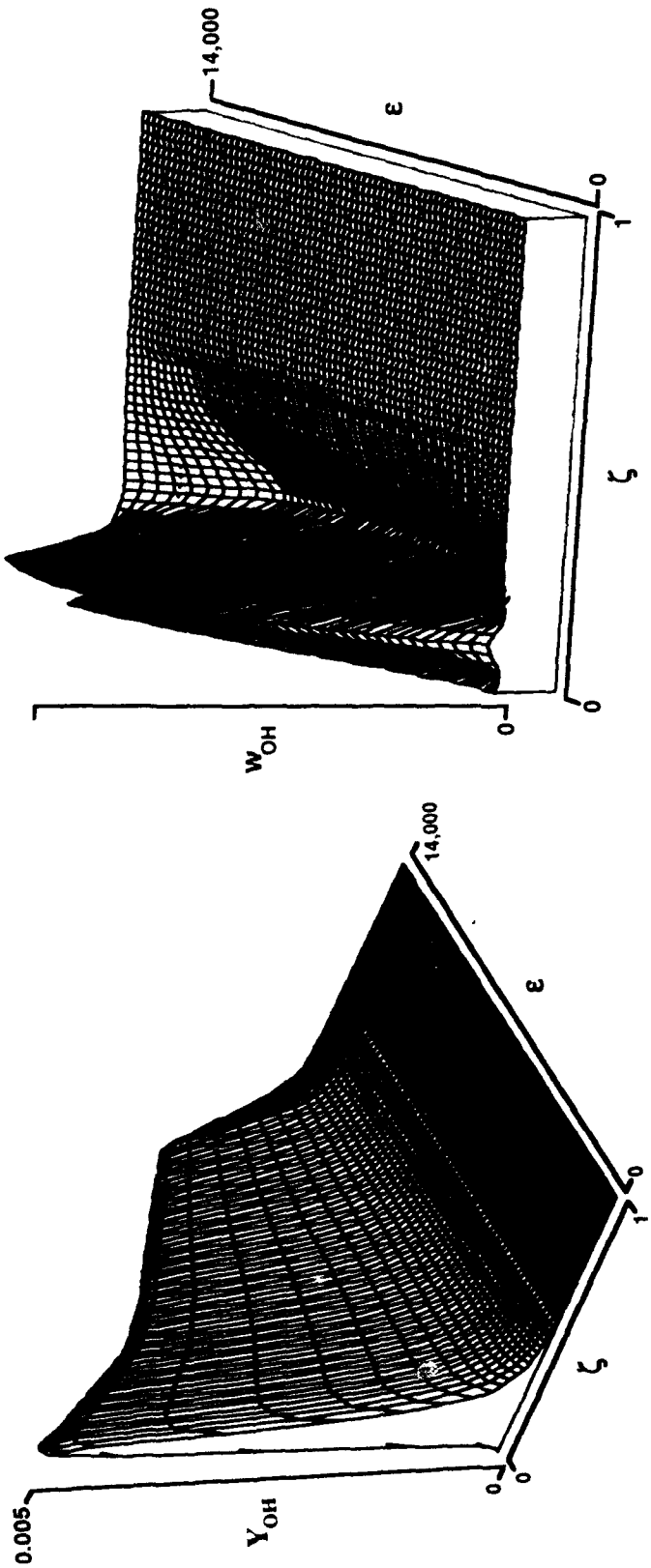

Fig. 3. OH library for a strained laminar diffusion and reaction layer between pure hydrogen and air, obtained from one-dimensional numerical calculations. *(a)* The OH mass fraction Y_{OH}. *(b)* The OH reaction rate w_{OH} in [mol/cm^3-s].

they represent inherently instantaneous reaction rate information.

Results are presented here for two different hydrogen-air turbulent jet diffusion flames, having the same far field Reynolds number (Re_δ = 14,000), but with conditions in the flame ranging locally from moderate to deep nonequilibrium conditions. The jet conditions for each of the cases considered are shown in Fig. 4, where the depth of nonequilibrium is indicated relative to the flame blowout limit for an unpiloted hydrogen-air turbulent jet diffusion flame. With the characteristic temperature approximately 1800 K, and $\nu \sim T^{1.5}$, this requires a cold-flow Reynolds number of 210,000 to produce a hot-flow conserved scalar field consistent with the Re_δ = 14,000 result in Fig. 1.

Our results have shown that Case (1) in Fig. 4 reproduces the equilibrium fields given in Buch et al (1992). Cases (2) and (3) are used here to examine the effects of chemical nonequilibrium. Case (2) produces a turbulent flame with a moderate level of nonequilibrium. It corresponds to a 10 mm exit diameter and an exit velocity (after correction for compressibility) of nearly 300 m/s. By comparison, Case (3) in Fig. 4 represents a turbulent flame under deep nonequilibrium conditions, with an exit diameter of 3 mm and exit velocity of 1 km/s, which can be seen to be only about slightly smaller than the flame blowout limit (Broadwell et al, 1984).

Figure 5 compares the OH mass fraction fields $Y_{OH}(\mathbf{x},t)$ obtained for Cases 2 and 3. Both are presented with the same color assignment scheme, as indicated on the color bar, in which pure blue denotes zero OH concentration, and colors increasing from blue to pure red denote linearly increasing OH mass fractions, clipped at 0.014. The fields are shown at four different downstream locations relative to the mean flame length L, centered at x/L = 0.25, 0.50, 0.75 and 1.0. The size of each panel has been correctly scaled and placed for its downstream location to give a proper indication of the structure of the flame. Notice that the resulting OH fields look remarkably similar to direct OH planar imaging measurements in turbulent jet flames.

In making comparisons between the two cases, as well as among different panels within each case, it is important to note that the degree of nonequilibrium varies not only between these cases, but also with the

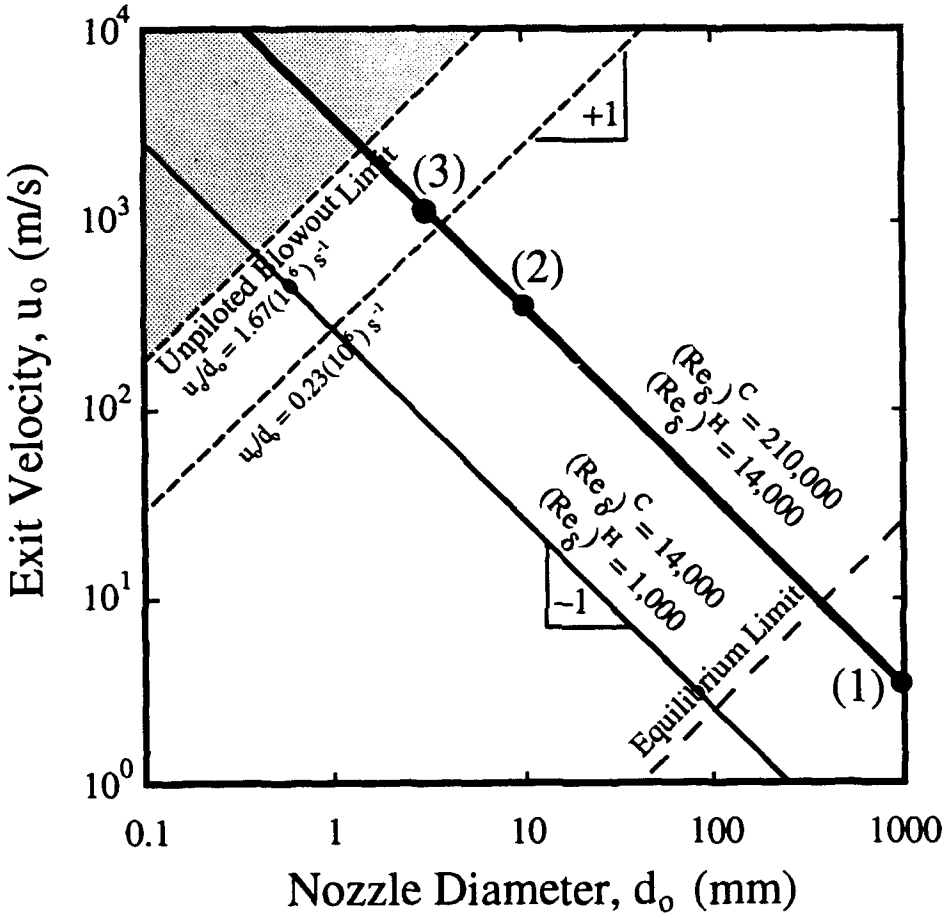

Fig. 4. Map of source conditions for turbulent hydrogen-air jet diffusion flames, showing depth of chemical nonequilibrium relative to the unpiloted blowout limit ($u_o/d_o = 1.67 \cdot 10^6\ s^{-1}$.). Solid line denotes far-field hot flow Reynolds number $Re_\delta = 14{,}000$ corresponding to cold flow $Re_\delta = 210{,}000$. Dashed lines denote constant global Damköhler number (u_o/d_o = const.) Shown are the conditions for three cases, giving (1) the equilibrium limit, (2) moderate nonequilibrium, and (3) deep nonequilibrium.

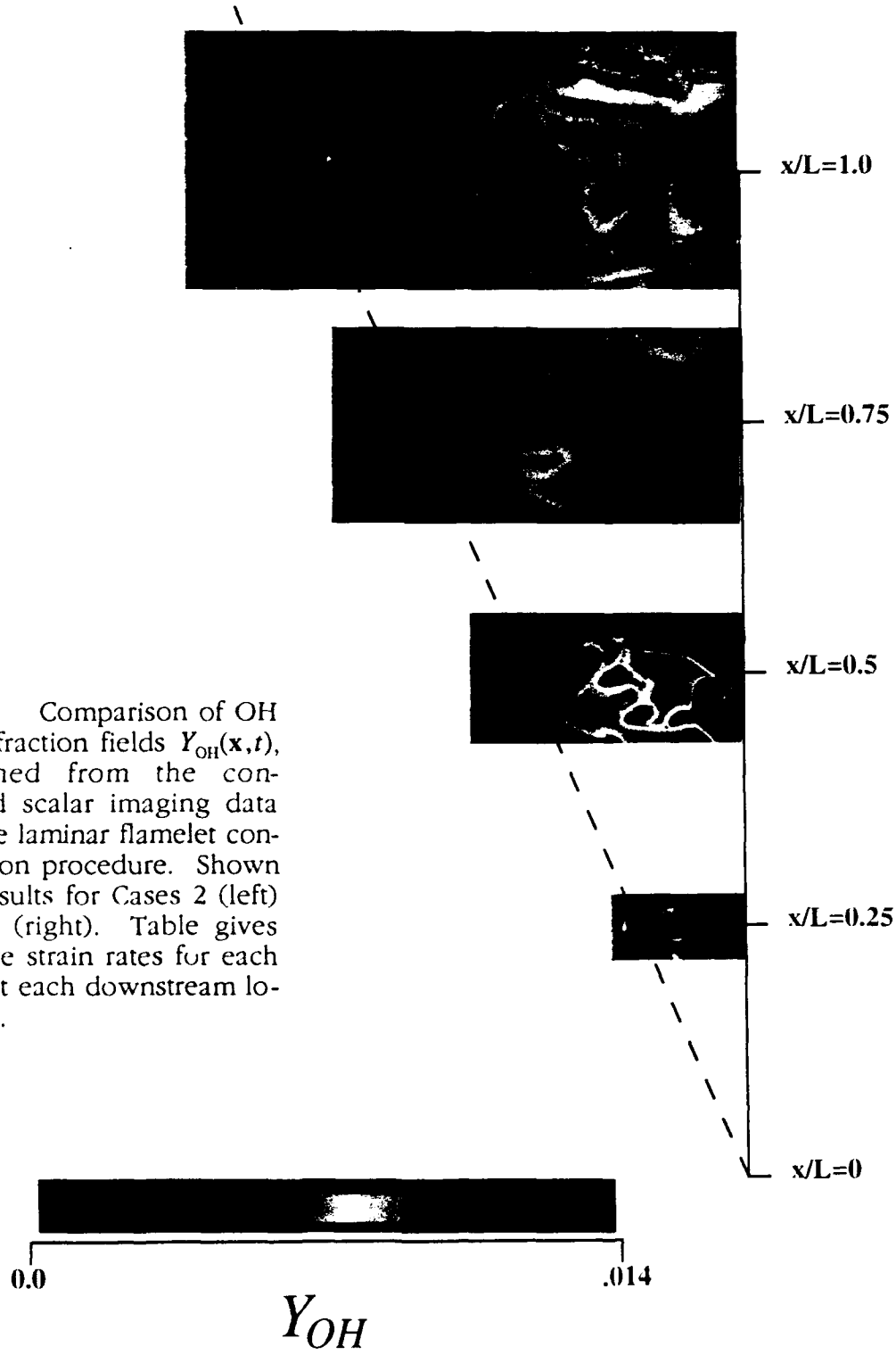

Fig. 5. Comparison of OH mass fraction fields $Y_{OH}(\mathbf{x},t)$, obtained from the conserved scalar imaging data via the laminar flamelet construction procedure. Shown are results for Cases 2 (left) and 3 (right). Table gives relative strain rates for each case at each downstream location.

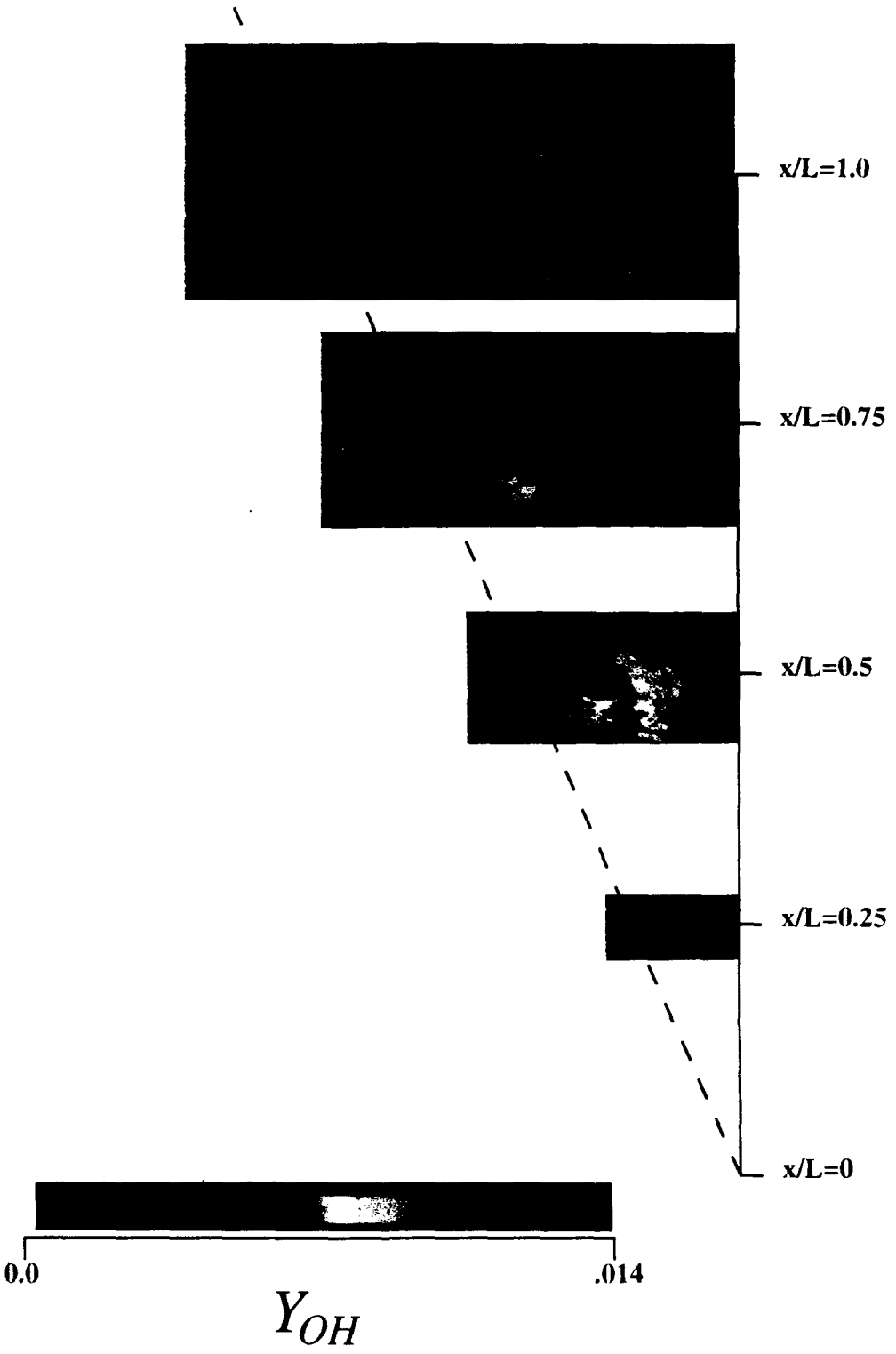
x/L=1.0
x/L=0.75
x/L=0.5
x/L=0.25
x/L=0
0.0
.014
Y_{OH}

downstream position x for any given case. Owing to the similarity scalings $\delta \sim x$ and $u \sim x^{-1}$ for this flow, the characteristic strain rates decrease like x^{-2}. Thus while the strain rates in each panel for Case 3 on the right are roughly 10 times higher than in the same panel for Case 2 on the left (see Fig. 4), the strain rates among the four downstream locations vary even more. For example, at x/L = 0.25 the strain rates are 16 times higher than the values at the flame tip. Within the two cases for which results are presented, the strain rates span a range of nearly 200, as indicated in the Table on the figure, which shows the local strain rates (inverse local Damköhler number) relative to the value at x/L = 0.25 in Case 2.

Differences evident in the OH concentration fields in Fig. 5 when comparing panels at the same downstream location for the two cases shown are due solely to the differing degrees of nonequilibrium. However, changes in the $Y_{OH}(\mathbf{x},t)$ field among panels corresponding to differing x/L values for the same case reflect changes in both the depth of nonequilibrium as well as changes in the scalar and dissipation rate values. For the jet similarity scalings, the scalar field values decrease with increasing distance from the jet source as $\zeta \sim x^{-1}$. Coupled with the linear increase in all length scales in the jet with increasing x, the resulting scalar dissipation field values decrease with distance from the jet source like $\nabla\zeta\cdot\nabla\zeta \sim x^{-4}$. These changes in both the $\zeta(\mathbf{x},t)$ and $\nabla\zeta\cdot\nabla\zeta(\mathbf{x},t)$ values with x/L will reassign each pixel in these data planes to a different point in the (ζ, $\nabla\zeta\cdot\nabla\zeta$) space in Fig. 2, and thereby to a different (ζ, ε) point in the flamelet library in Fig. 3. Thus, in examining the results in Fig. 5, as well as those in Figs. 6–8, it must be borne in mind that comparisons made among different cases but at the same downstream location show the effects of the degree of nonequilibrium only, while comparisons made at different downstream locations within the same case demonstrate the effects of both nonequilibrium level and changes in the scalar field values. However, by arranging the results in the manner shown, it is possible to separate the changes due solely to the degree of nonequilibrium from those due to changes in the conserved scalar and dissipation rate values.

With this we can now meaningfully understand the nonequilibrium structure of the OH mass fraction fields in Fig. 5. Note firstly that, within Case 2, there is a fundamental change in the structure of the OH concentrations with

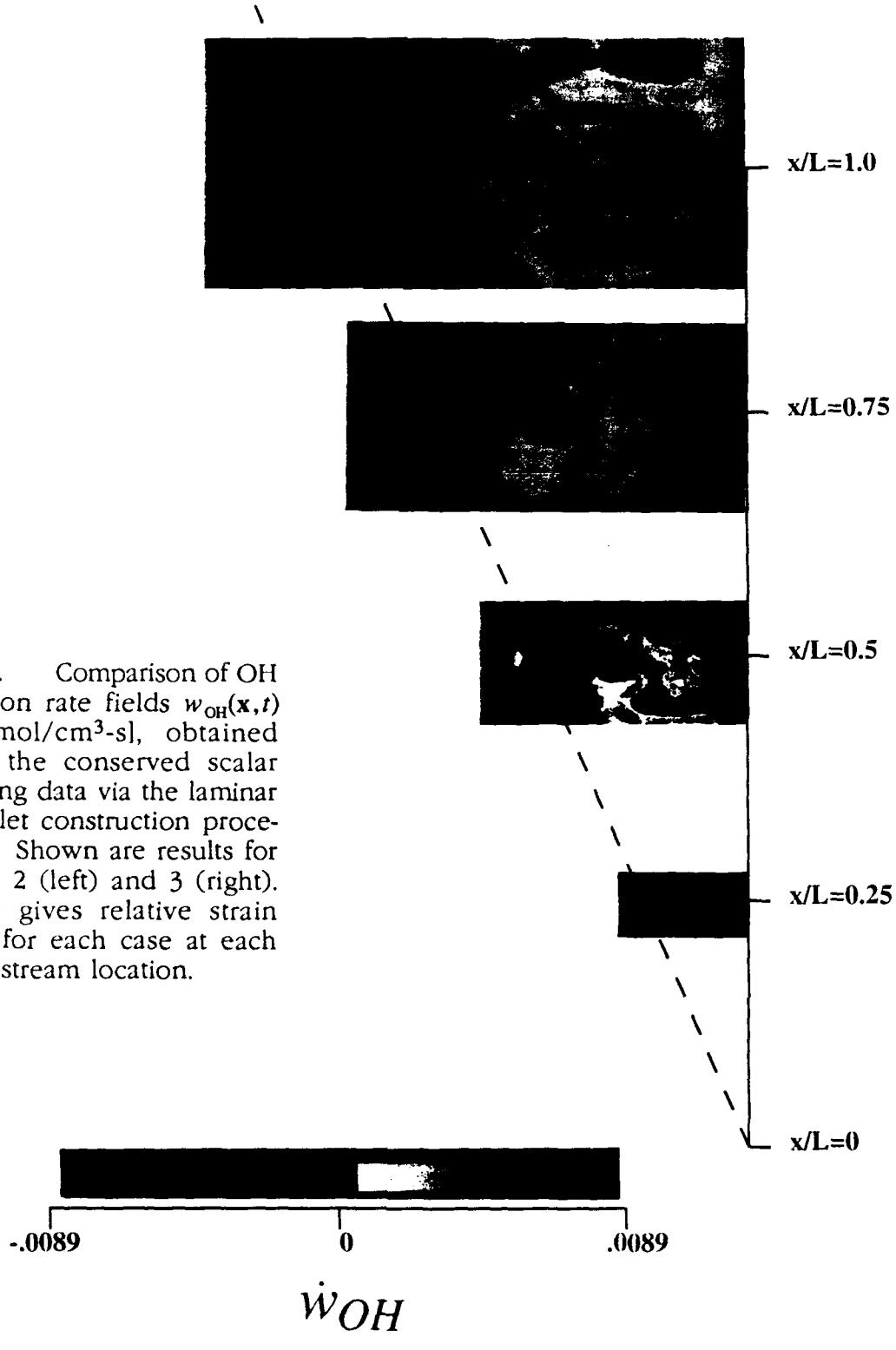

Fig. 6. Comparison of OH reaction rate fields $w_{OH}(\mathbf{x},t)$ in [mol/cm^3-s], obtained from the conserved scalar imaging data via the laminar flamelet construction procedure. Shown are results for Cases 2 (left) and 3 (right). Table gives relative strain rates for each case at each downstream location.

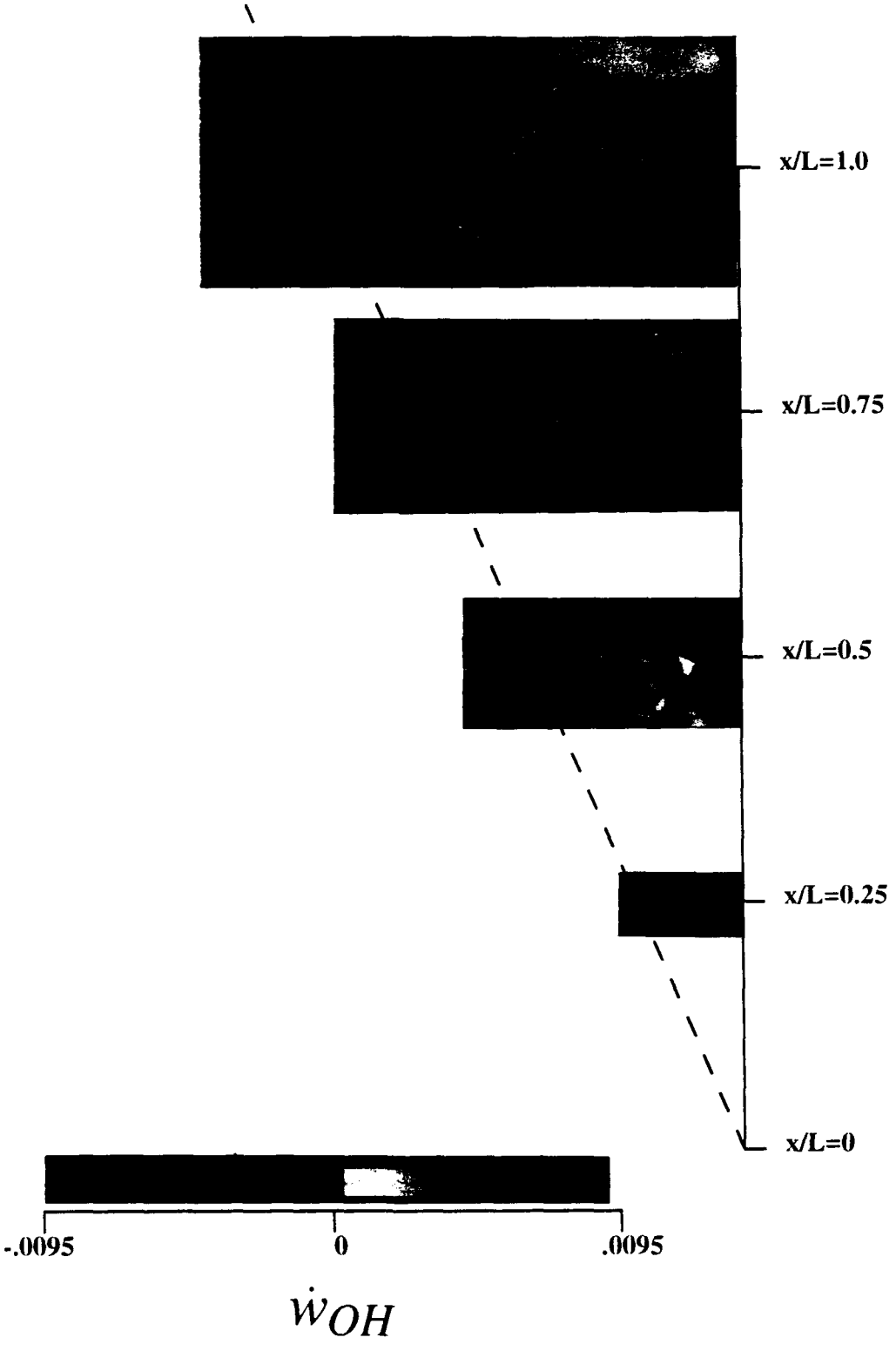
x/L=1.0
x/L=0.75
x/L=0.5
x/L=0.25
x/L=0
-.0095
0
.0095
$\dot{w}_{OH}$

increasing downstream distance from the nozzle. In particular, the layers containing high OH concentrations evident at the flame tip, and to a lesser extent also evident at x/L = 0.75, are virtually gone at x/L = 0.50, and by x/L = 0.25 the OH concentration field shows only featureless blobs of high OH values. Case 3, by comparison, shows little evidence of any layer-like structure in the OH field anywhere in the flame. These fields resemble far more the blobs seen at x/L = 0.25 and 0.50 in Case 2. Indeed, the strain rates in the four panels shown for Case 3 are all roughly comparable to or higher than those at x/L = 0.25 in Case 2. Even at the flame tip in Case 3, the strain rates are still nearly as high as those at x/L = 0.25 in Case 2. Similarly, when we compare panels at the same x/L values between Cases 2 and 3, there is a clear tendency for the layers present in Case 2 to change to blobs owing to the increased depth of nonequilibrium.

What is remarkable, however, is that despite the wide variations in the OH concentration field structure seen in Fig. 5 with changing downstream position and with global Damköhler number, all of these fields ultimately resulted from the same conserved scalar data plane shown in Fig. 1. Thus even the broad regions of high OH concentration in Case 3, and at small x/L in Case 2, all resulted from a simple layer-like structure in the scalar dissipation rate field in Fig. 1b. This appears to have considerable potential for organizing the wide variations apparent in the OH concentration fields into a single underlying canonical structure. Evidently, the simple layer-like structure in Fig. 1 suffices to reconcile both the layer-like and broad OH zones appearing in Fig. 5 under differing conditions of nonequilibrium and locations in the flame.

Figure 6 now shows the OH reaction rate field for the same two cases. Black now corresponds to zero reaction rate, while yellow through red correspond to increasing OH formation rates, and blue through green denote increasing rates of consumption of OH, as indicated by each color bar. Black regions inside the flame correspond to strained out areas. There are two main points to note here. First, there is a fair correspondence between the OH concentration and reaction rate fields up to about x/L = 0.5, but beyond that the OH mass fraction gives only a rather poor indication of the reaction zone structure. Second, while there are clearly reactions occurring in blobs in parts of the flame, there appears to be a persistent layer-like structure in the reaction rate field, even when the OH concentration field gives no evidence of it, as at x/L

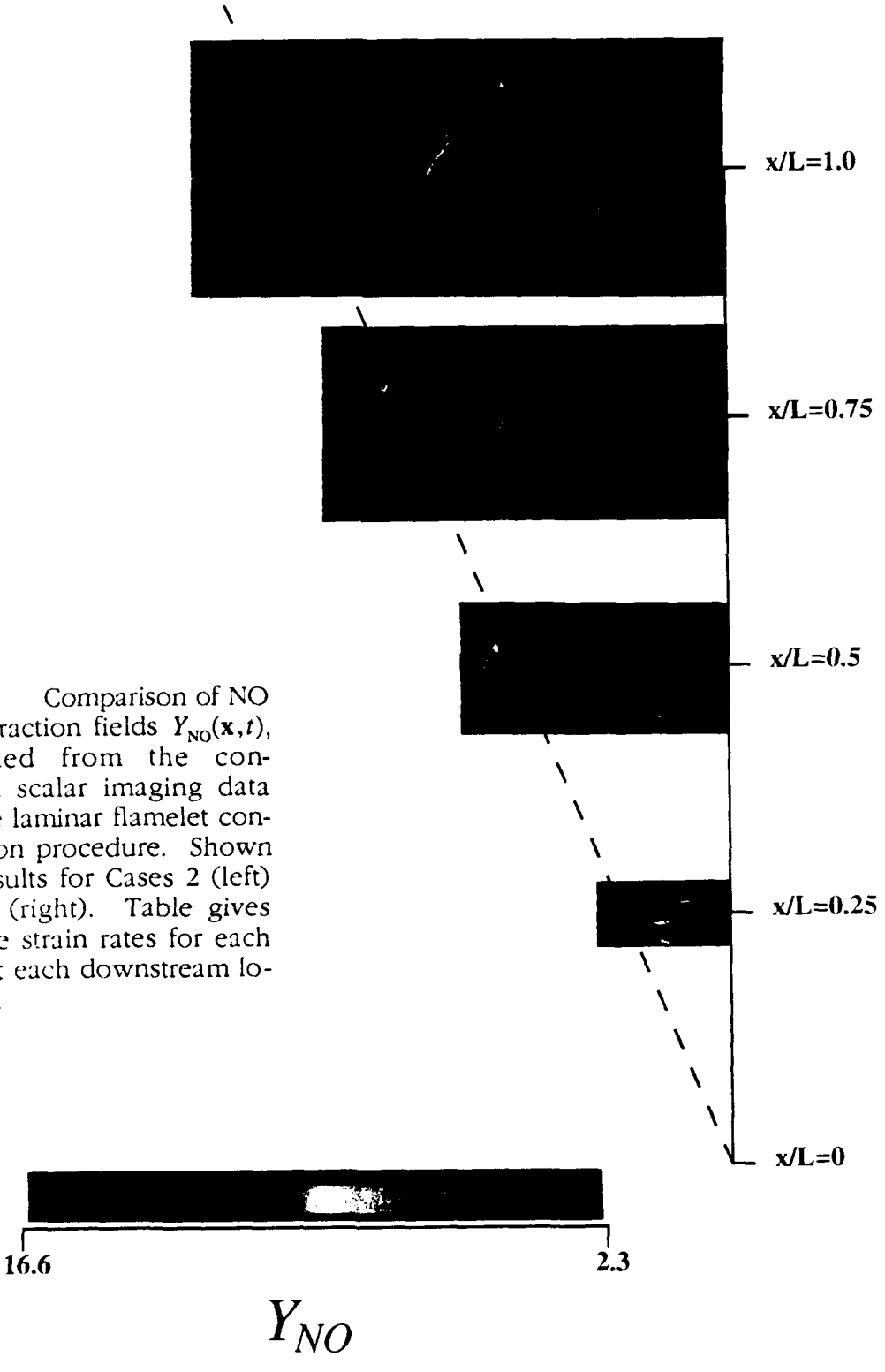

Fig. 7. Comparison of NO mass fraction fields $Y_{NO}(\mathbf{x},t)$, obtained from the conserved scalar imaging data via the laminar flamelet construction procedure. Shown are results for Cases 2 (left) and 3 (right). Table gives relative strain rates for each case at each downstream location.

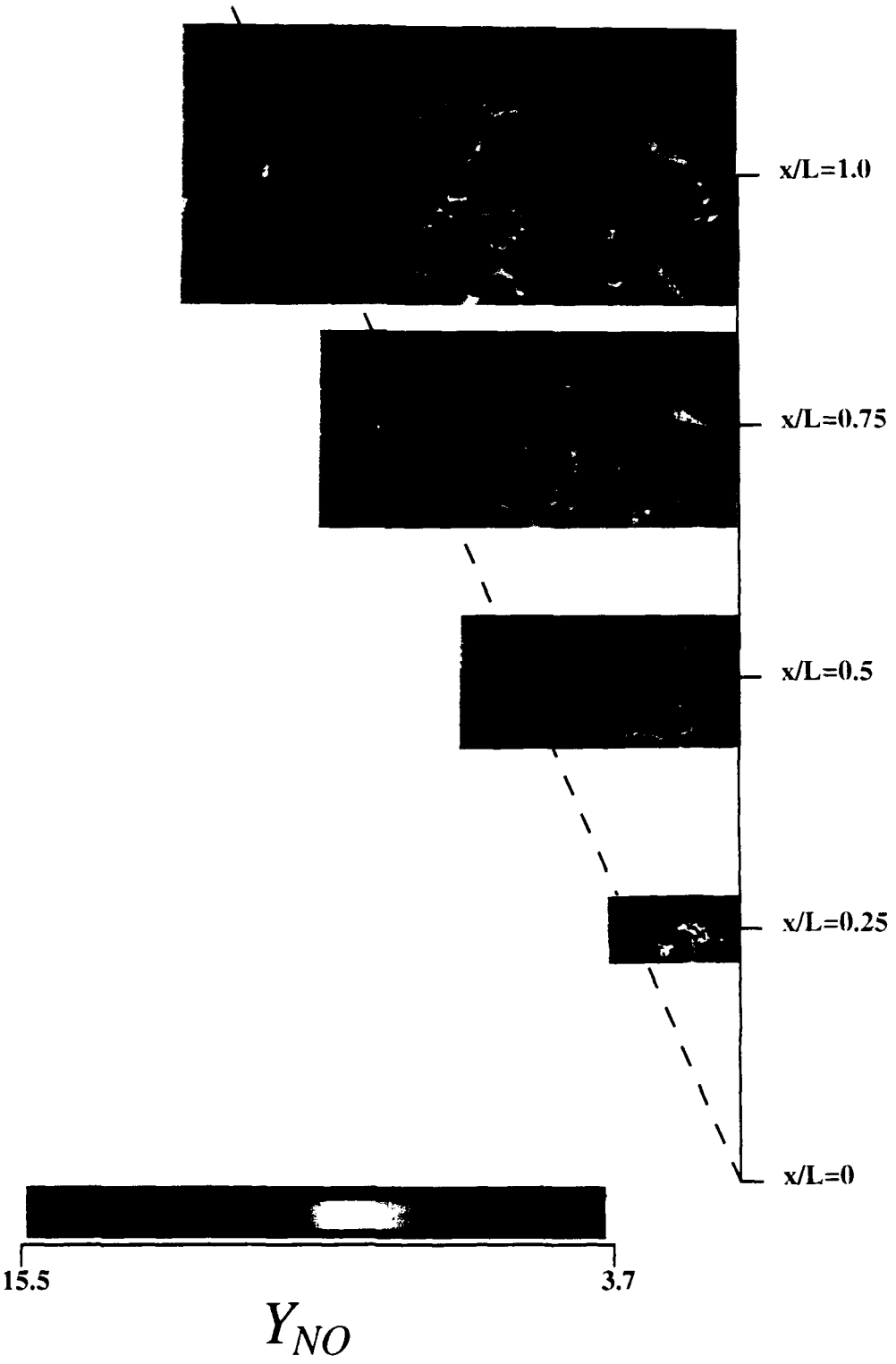
x/L=1.0
x/L=0.75
x/L=0.5
x/L=0.25
x/L=0
15.5
3.7
Y_{NO}

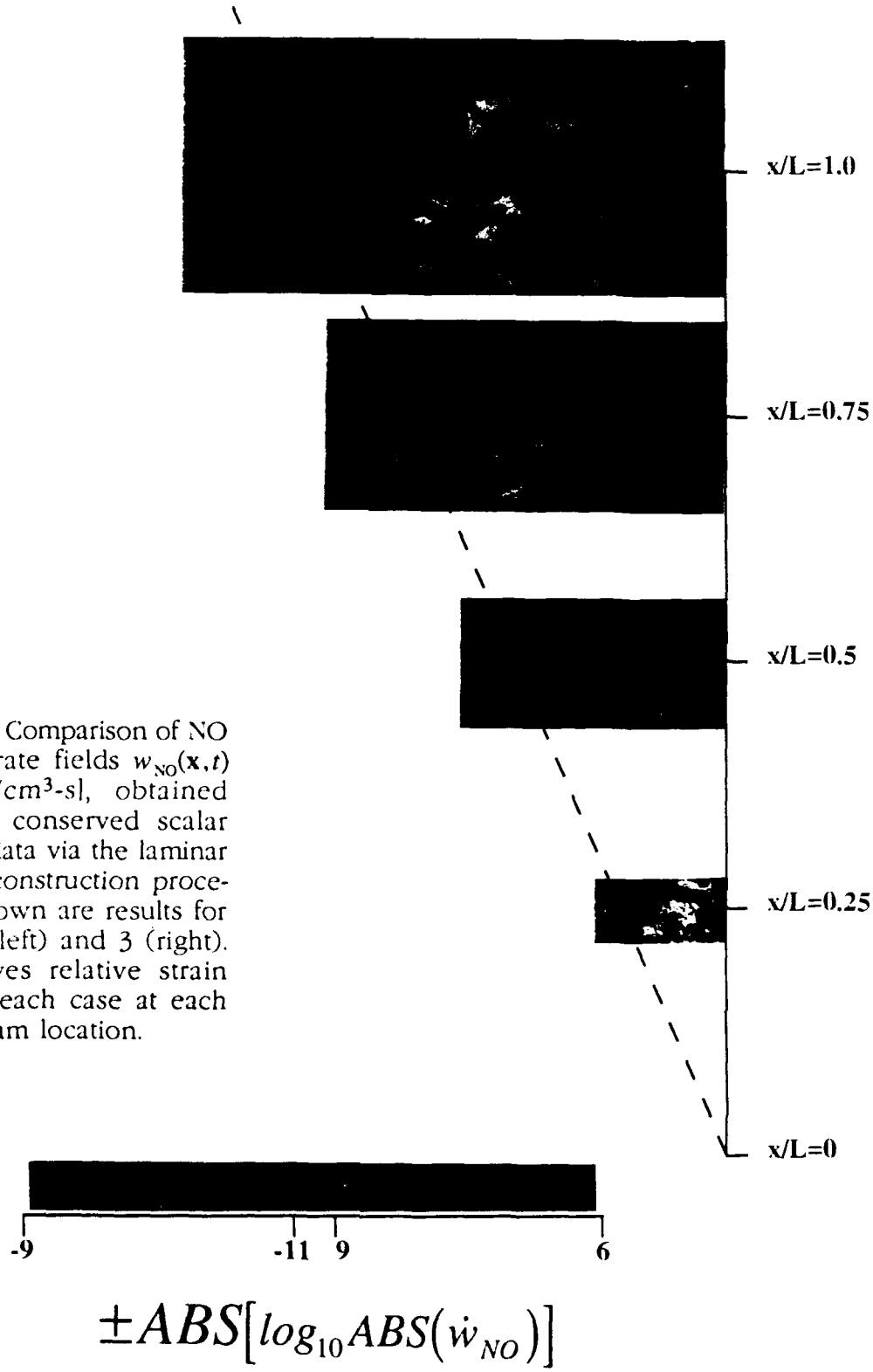

Fig. 8. Comparison of NO reaction rate fields $w_{NO}(\mathbf{x},t)$ in [mol/cm^3-s], obtained from the conserved scalar imaging data via the laminar flamelet construction procedure. Shown are results for Cases 2 (left) and 3 (right). Table gives relative strain rates for each case at each downstream location.

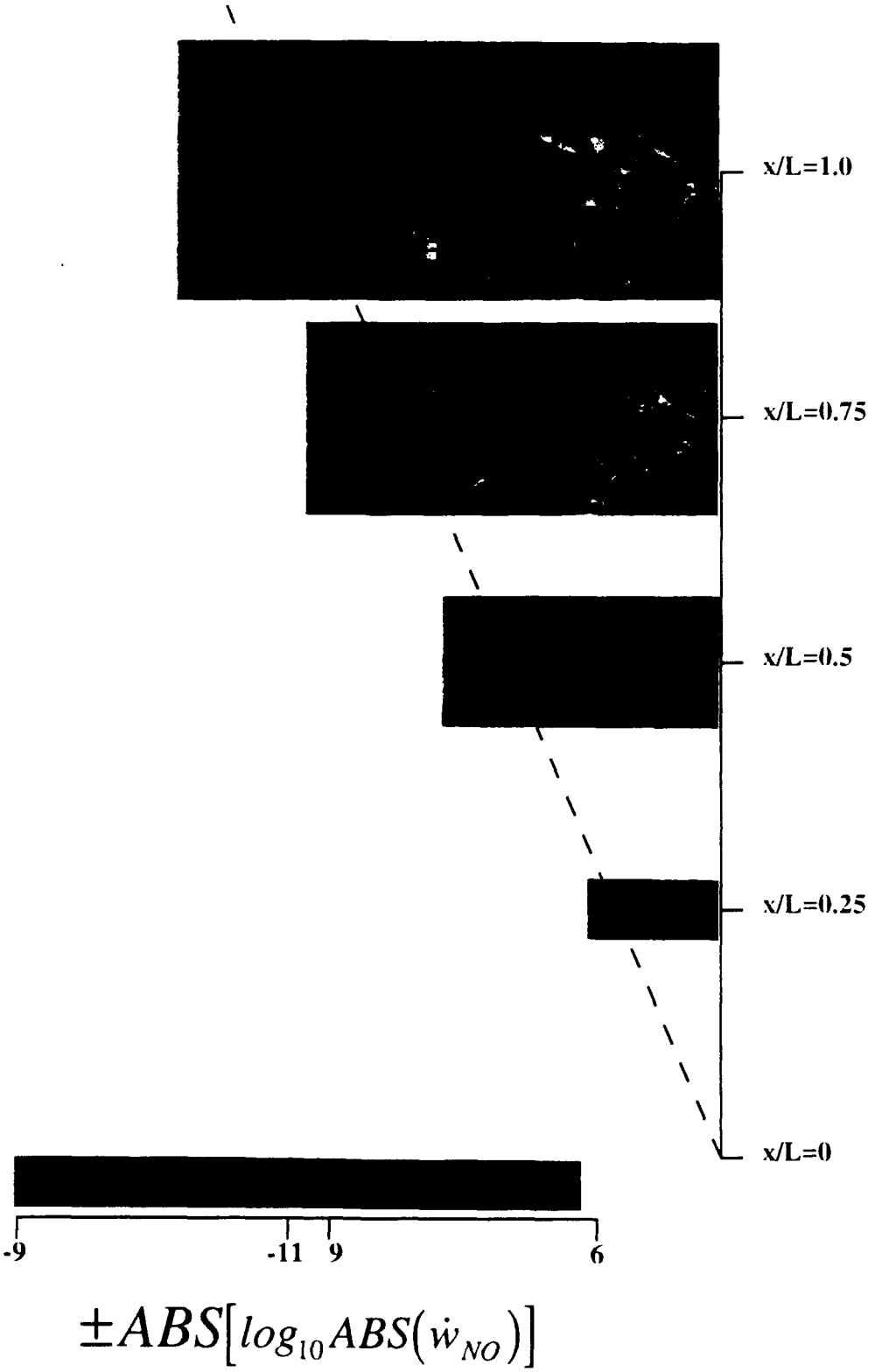
x/L=1.0
x/L=0.75
x/L=0.5
x/L=0.25
x/L=0
-9
-11
9
6
$\pm ABS[log_{10} ABS(\dot{w}_{NO})]$

= 1 in Case 3.

Figures 7 and 8 show corresponding results for the NO mass fraction and reaction rate fields. (Our work on nitric oxide in turbulent diffusion flames also involves funding from the Gas Research Institute.) Here it is necessary to plot these in logarithmic form, owing to the wide range of concentrations and reaction rates present. Similar patterns can be seen as the degree of nonequilibrium increases and the position in the flame changes. In this case, however, the relatively broad region of ζ covered by the NO concentrations, coupled with the strong dependence on the dissipation rate, leads to features not seen in the OH fields in Figs. 5 and 6.

The flamelet approach demonstrated here for constructing instantaneous species concentration and reaction rate fields under increasing degrees of nonequilibrium chemistry allows considerable insights to be gained into the structure of turbulent flames. The results show that the wide variations apparent in the structure of OH concentration fields, both in the results presented here and in direct OH imaging measurements, can be reconciled into a single underlying canonical structure. In particular, the simple layer-like structure in the scalar and dissipation rate fields seen in Fig. 1 suffices to explain both the layer-like and broad OH zones appearing in Fig. 5 under differing conditions of nonequilibrium and at various locations in the flame. Analysis of this type on our high-resolution conserved scalar imaging data are providing new insights into the structure of chemical reactions in turbulent combustion.

1.3. Topology and Scaling Properties of Scalar Dissipation Layers

Molecular mixing of dynamically passive conserved scalar quantities in turbulent flows plays a central role in an enormous range of practical problems. The mixing process can be formally quantified in terms of the conserved scalar field $\zeta(\mathbf{x},t)$ and the associated instantaneous scalar energy dissipation rate field $(ReSc)^{-1}\nabla\zeta\cdot\nabla\zeta(\mathbf{x},t)$. This aspect of our work involves results obtained using a laser imaging diagnostic specifically designed for very highly resolved, four-dimensional measurements of the full space- and time-varying conserved scalar field $\zeta(\mathbf{x},t)$ and the associated scalar energy dissipation rate field $\nabla\zeta\cdot\nabla\zeta(\mathbf{x},t)$ in turbulent flows. Measurements with this technique have been obtained in the

self-similar far field of axisymmetric turbulent jets at outer-scale Reynolds number $Re_\delta \equiv (u\delta/\nu)$ as high as 6000, with the resolution achieved being finer than the local strain-limited molecular diffusion scale λ_D. Since the imaged region of the flow is quite small in comparison with the local outer scale δ, and comparable to the inner scale λ_ν, of the flow, the resulting measured turbulent scalar field fine structure should be essentially independent of the Reynolds number and the flow, and depend only on the Schmidt number. In this sense, many features of the fine structure captured within our four-dimensional data space should to a large degree be generic to large Schmidt number mixing in all high Reynolds number turbulent flows.

The measurements are of the aqueous concentration of a dynamically passive dilute laser fluorescent dye (disodium fluorescein) carried by one of the fluids in the self-similar far field of an axisymmetric turbulent jet. The dye mixture fraction is a conserved scalar variable for which $Sc \approx 2075$. This mixture fraction is measured repeatedly in time throughout a small three-dimensional volume in the flow (see Fig. 1) by imaging the laser induced fluorescence from dye-containing fluid in the path of a laser beam rapidly swept in a raster fashion through the volume onto a high-speed planar photosensitive array. A pair of very low inertia, galvanometric mirror scanners are used to synchronously sweep a collimated laser beam in a raster scan fashion through the desired volume in the flow field. The resulting laser induced fluorescence intensity is measured with a 256 × 256 imaging array, having center-to-center pixel spacings of 40μm. The array is synchronized to the same clock that drives the scanners, and can be driven at variable pixel rates up to 11 MHz, allowing measurement of successive data planes at a continuous rate in excess of 140 planes per second. The fluorescence data from the array is serially acquired through a programmable digital port interface, digitized to 8-bits digital depth, then routed into a 16 MB high-speed dual-ported data buffer from which it can be continuously written in real time to a 3.1 GB high-speed parallel transfer disk rank. The overall sustained data throughput rate to the disks, accounting for all line and frame overhead cycles, is up to 9.3 MB/sec. The 3.1 GB disk capacity can accommodate more than 50,000 such measured 256 × 256 spatial data planes within the four-dimensional spatio-temporal data space. The spatial separation between adjacent points within each data plane, and between adjacent data planes within each data volume, is smaller than the local strain-limited molecular

diffusion lengthscale λ_D of the scalar field. Similarly, the temporal separation between adjacent data planes within each data volume, and between the same data plane in successive data volumes, is shorter than the local molecular diffusion scale advection time λ_D/u. This resolution, together with the high signal quality attained, allows accurate differentiation of the measured conserved scalar data in all three space dimensions and in time to determine the components of the local instantaneous scalar gradient vector field $\nabla\zeta(\mathbf{x},t)$ at every point in the data space. From this, the true instantaneous scalar energy dissipation rate field $\nabla\zeta\cdot\nabla\zeta(\mathbf{x},t)$ can be determined.

Since the principal interest is in obtaining the scalar energy dissipation rate field from the measured conserved scalar field via direct differentiation of the data, the central issue is the spatial and temporal resolution achieved by the measurements. From the measured thickness of the imaged portion of the laser beam, together with the pixel size and the image ratio of the measurements, the volume in the flow $(\Delta x\cdot\Delta y\cdot\Delta z)$ imaged onto each pixel can be determined. Furthermore, for the pixel clock rates used, the time Δt between acquisition of successive data planes within each spatial data volume, and the time ΔT between the same data plane in successive data volumes, can also be determined. To assess the resulting relative resolution achieved, these smallest spatial and temporal scales discernible in the data must be compared with finest local spatial and temporal scales on which gradients in the conserved scalar field can be sustained in the flow. In particular, for local diffusion of vorticity in the presence of a time-varying strain rate ε, the competing effects of strain and diffusion establish an equilibrium strain-limited vorticity diffusion layer thickness $\lambda_\nu \sim (\nu/\varepsilon)^{1/2}$, closely related to the Kolmogorov scale, giving the finest scale on which spatial gradients in the strain rate and vorticity fields can be locally sustained in the flow (e.g. Burgers 1948; Townsend 1951). A similar competition between the effects of strain and molecular diffusion of the conserved scalar establishes a local strain-limited molecular diffusion layer thickness $\lambda_D \sim (D/\varepsilon)^{1/2}$, related to the Batchelor scale and giving the smallest scale on which spatial gradients in the conserved scalar field can be sustained by the flow. The ratio of the vorticity and scalar diffusivities, ν and D respectively, establishes the relation between these two scales as $\lambda_D \approx \lambda_\nu\cdot Sc^{-1/2}$. Note that, with the highest strain rates occurring locally in the flow scaling as $\varepsilon \sim (u/\delta)\cdot Re^{1/2}$, the strain-limited diffusion scale in the conserved scalar field is $(\lambda_D/\delta) \sim Sc^{-1/2}\, Re^{-3/4}$. The most

recent measurements give the resulting proportionality constant as 11.2.

Figure 1 shows the conserved scalar data in a typical 256 × 256 spatial data plane. All quantities presented have been nondimensionalized by the inner-scale reference values $l^* \equiv \lambda_v$, $u^* \equiv (\nu/\lambda_v)$ and the local mean scalar value $\zeta^* \equiv \zeta_m$. It also shows the true scalar energy dissipation rate field $\nabla\zeta\cdot\nabla\zeta(\mathbf{x},t)$ obtained by direct differentiation of the data in the three adjacent scalar planes centered on each plane. Linear central difference approximations have been used to evaluate the three components of the scalar gradient vector field $\nabla\zeta(\mathbf{x},t)$, with no explicit smoothing or filtering of the results. Owing to the wide range of resulting dissipation rates, the logarithmic compression $log_e\,\nabla\zeta\cdot\nabla\zeta(\mathbf{x},t)$ in Fig. 1 allows the structure at low dissipation rates to be examined. Our previous work on these fine structure maps of the instantaneous scalar dissipation field has clearly shown that essentially all of the molecular mixing occurs in thin sheet-like layers of the type described by Burgers and Townsend for the vorticity field. The internal structure of the molecular mixing within the layers apparent in these measurements can also be examined from our measurements, and confirm that strain-limited solutions of the Burgers and Townsend form give a remarkably accurate description of the true scalar energy dissipation profiles within these layers.

Our work with these measurements and the resulting data during the past twelve months has focused on analyses using three different analytical approaches. These include (1) layer separation distributions, (2) critical point analyses, and (3) multifractal topology studies. Our interests are principally in the topology which the scalar dissipation layers assume as a result of their repeated stretching and folding by the turbulent strain rate and vorticity fields. The aim is to obtain measurements of the scalings which this topology satisfies, and relate these to the dynamics of the "turbulent cascade" represented by this stretching and folding process. We are motivated by recent successes in comparatively simple two-dimensional chaotic flows (Ottino 1992; Muzzio, Meneveau, Swanson & Ottino 1992), where a periodic stretching and folding of the scalar layers leads to scalings for the distribution of dissipation layer separations that can be reconciled with simple physical arguments. These analyses suggest a lognormal distribution for the distribution of layer separations, though on quite different (and more rigorous) grounds than the

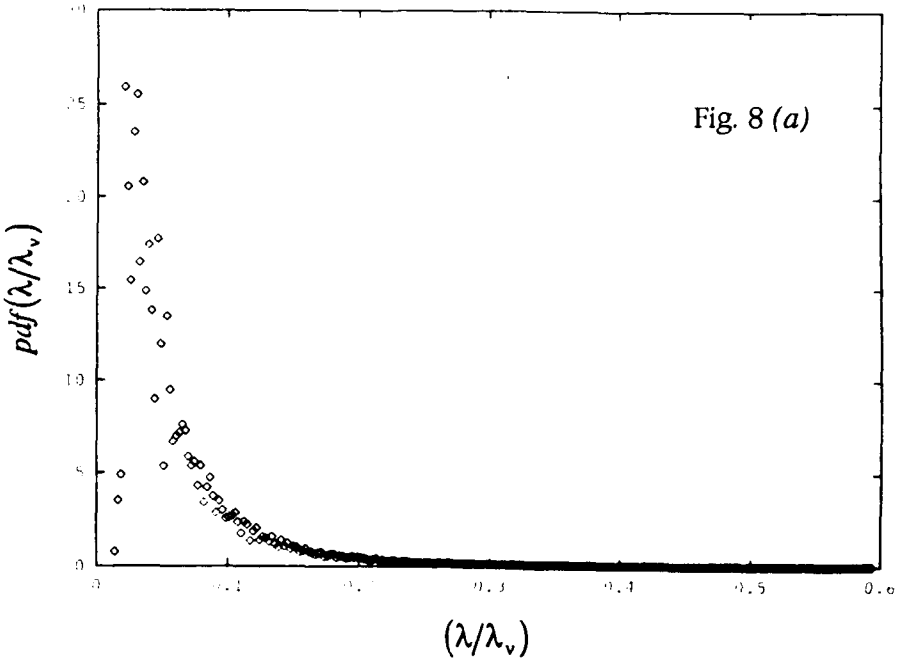

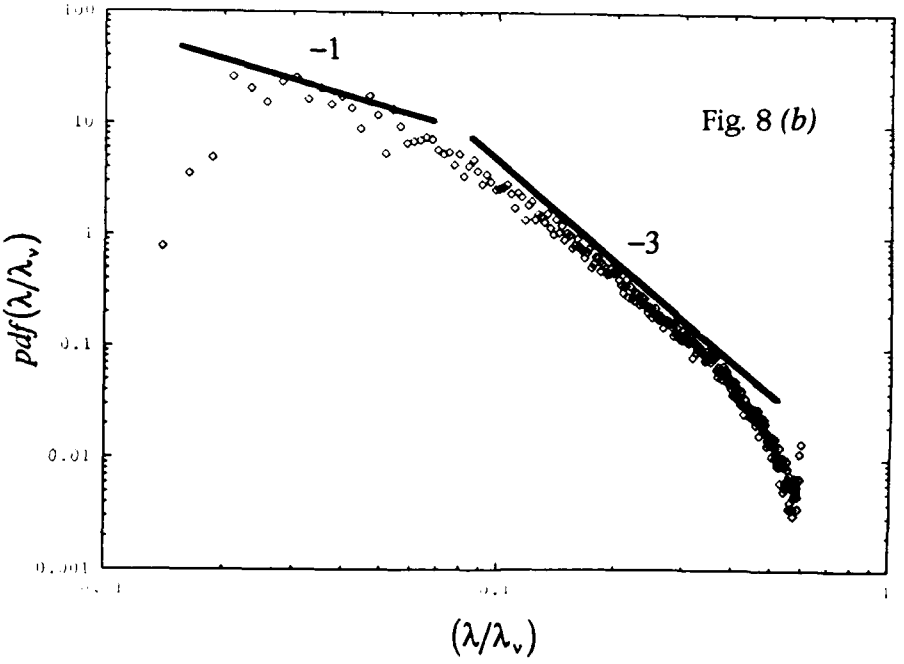

Fig. 9. The measured distribution of the scalar dissipation layer separation distances λ/λ_v, obtained from three-dimensional spatial data volumes of the type shown in Fig. 1. Note the quasi-lognormal form obtained for small layer separation values, and the non-lognormal form found at larger separation values. (a) The linear version. (b) The logarithmic version.

classical lognormal predictions for other single-sided quantities in turbulence. From the three-dimensional spatial character of the turbulent dissipation rate field in any given data volume, we construct the surface of local layer-normal dissipation maxima. We can then compute the distribution of dissipation layer separations λ/λ_v. The roughly lognormal form appears consistent with the scalings obtained in the simple periodic flows, but for large layer separations we find deviations from this simple scaling. Our analyses of these differences is not yet complete, but they appear to be due to differences between turbulence in closed and open systems. In particular, in an open system like the turbulent jet (and other practical free shear flows), there is a continual entrainment of dissipation-free fluid into the flow. This dissipation-free fluid is subsequently intertwined with the dissipation layers in the turbulent flow, and continually introduces regions with large dissipation layer separation distances. No such mechanism exists in a closed turbulent flow, since there is no entrainment of dissipation-free fluid. As a consequence, the lognormal distribution (which does not take into account such entrainment) produces a relatively good fit to the distribution for small separations. For large values it would not be expected to give accurate predictions, and that is indeed seen to be the case. At these larger values, the scaling appears to be consistent with simple volume-preserving constraints that play a dominant role in the entrainment process.

These analyses play a key role in developing a practical model for reacting turbulent flows to aid in development of new airbreathing propulsion systems. In particular, the two-parameter nonequilibrium reaction chemistry formulation in §1.2 requires joint information about the conserved scalar and its dissipation rate. When that formulation is coupled with these simple scalings for the dissipation layer separations, it appears to be possible to predict the relative dominance of layer-like reaction zone structure versus broad distributed reaction zone structure. Moreover, it appears possible to fold this information into a new class of sub-grid scale models for reacting flows, in which the computed scales impose the local outer scale strain field on the distribution of layer separations. This scales the distribution of local strain rates at the subgrid scale, which in turn coupled with the nonequilibrium chemistry formulation to allow prediction of species mass fractions and reaction rates for complex reaction chemistry.

2. Personnel

The following personnel were associated with this research effort during the report period.

A. Faculty

Dr. Werner J.A. Dahm; Associate Professor, The University of Michigan, Department of Aerospace Engineering, Ph.D., US Citizen.

B. Graduate Students

Southerland, K.B.; Graduate Student, The University of Michigan, Department of Aerospace Engineering, Ph.D. program, US Citizen. Mr. Southerland is the principal graduate student research assistant working on this grant, and he is fully supported through his work on the grant.

Bish, E.; The University of Michigan, Department of Aerospace Engineering, Ph.D. program, US Citizen. Mr. Bish is 85% supported through a DoEd Fellowship; he receives 15% support ($200/month + 1 summer month) from his work on this grant.

Frederiken, R.E.; The University of Michigan, Department of Aerospace Engineering, Ph.D. program, US Citizen. Mr. Frederiken is 80% supported through a Departmental Teaching Assistantship; he receives 10% support ($100/month + 1.5 summer months) from his work on this grant. Application to the DoD ASSERT Program has been made to allow him to work full-time on this project with funds outside the grant budget.

C. Post-Doctorates

Buch, Kenneth A., Jr.; Michigan, Aerospace Engineering, Ph.D., US Citizen. During the time spanned by this worksheet, Dr. Buch worked partly on this grant from June 1991 through December 1991. He received approximately 20% of his support for his work on this grant.

3. Publications

The following publications have resulted during this reporting period in part from the research work undertaken in this research program into the structure of chemical reactions in turbulent flows.

1. Dahm, W.J.A. & Bish. E. (1992) "High resolution measurements of molecular transport processes in turbulent combustion," Turbulence and Molecular Processes in Combustion, Elsevier, in press.

2. Dahm, W.J.A., Southerland, K.B. and Buch, K.A. (1991) Four-dimensional laser induced fluorescence measurements of conserved scalar mixing in turbulent flows, Applications of Laser Techniques to Fluid Mechanics, 3–18, R. Adrian, Ed., Springer Verlag, Berlin.

3. Dahm, W.J.A. & Southerland, K.B. (1992) "Quantitative, four-dimensional, laser induced fluorescence imaging studies of scalar mixing in turbulent flows," Flow Visualization 6, 243-247, Springer-Verlag, Berlin.

4. Buch, K.A., Dahm, W.J.A., Dibble, R.W. & Barlow, R.S. (1992) "Equilibrium structure of reaction rate fields in turbulent jet diffusion flames," to appear in Proceedings of the 24th International Symposium on Combustion, The Combustion Institute, Pittsburgh.

5. Dahm, W.J.A. (1992) "Experimental studies of the fine scale structure of mixing in turbulent flows," Proceedings of the 13th Symposium on Turbulence, The University of Missouri (Rolla), Rolla, MO.

4. Presentations

The following presentations have resulted during this reporting period in part from the research work undertaken in this research program into the structure of chemical reactions in turbulent flows.

1. Fully-Resolved, Four-Dimensional, Laboratory Measurements of the Fine Scale Structure of Turbulent Flows - Invited Seminar, Mechanical Engineering Department, Purdue University, West Lafayette, IN, September 1991.

2. Fully-Resolved, Four-Dimensional, Laboratory Measurements of the Fine Scale Structure of Mixing in Turbulent Flows - Invited Seminar, Mechanical Engineering

Department, University of California at Davis, Davis, CA, February 1992.

3. Experimental Studies of the Fine Structure of Mixing in Turbulent Flows - Invited Seminar, Mechanical, Aerospace & Nuclear Engineering Department, University of California (Los Angeles), March 1992.

4. Small Scale Structure of Turbulent Diffusion Flames - Invited Lecture, 19th Meeting of the Sandia Technical Group on Aerothermochemistry of Reacting Flows, Lawrence Berkeley Laboratories, CA, April 1992.

5. Structure of Mixing and Reactions in Turbulent Flows - Invited Seminar, High Temperature Gas Dynamics Laboratories, Mechanical Engineering Department, Stanford University, Stanford, CA, April 1992.

6. Equilibrium Structure of Chemical Reaction Rate Fields in Turbulent Diffusion Flames - 24th International Symposium on Combustion, The University of Sydney, Sydney, Australia, June 1992.

7. Experimental Studies of the Fine Scale Structure of Mixing in Turbulent Flows - Invited Lecture, Thirteenth Symposium on Turbulence, Rolla, MO, September 1992.

8. Quantitative, Four-Dimensional, Laser Induced Fluorescence Imaging Studies of Scalar Mixing in Turbulent Flows - Sixth International Symposium on Flow Visualization, Yokohama, Japan, October 1992.

9. High Resolution Measurements of Molecular Transport Processes in Turbulent Combustion - Invited Lecture, 6th Toyota Symposium on Turbulence and Molecular Processes in Combustion, Nagoya, Japan, October 1992.

10. Modeling NOx in Turbulent Diffusion Flames - Invited Presentation, 2nd International Workshop on NOx in Natural Gas Flames, Orlando, FL, November 1992.

11. Laboratory Studies of the Fine Scale Structure of Turbulent Flows: $Sc \gg 1$, $Sc \approx 1$, and Implications for Reacting Flows - Invited Seminar, Theoretical Division TA-3, Los Alamos National Laboratories, December 1992.

5. Research-Related Interactions

Interactions related to this research effort during the reporting period have been underway with personnel at the Combustion Research Facility (CRF) at Sandia National Laboratories (Livermore, CA); at ETH–Zürich in Switzerland; and at Nagoya University in Japan. The Principal Investigator conducted a five-

month sabbatical visit to the CRF from January – May 1992 during which measurements of OH concentrations were made in conjunction with Dr. P.H. Paul for comparison with our flamelet analysis predictions. Measurements were also planned for four-dimensional Rayleigh imaging of a conserved scalar field in high Reynolds number turbulent mixing. An on-going interaction with the Swiss Federal Institute of Technology (ETH) in Zürich has been aimed at setting up a similar diagnostic system as ours in their laboratories for additional measurements. A graduate from our research group has been sent to ETH on a postdoctoral assignment for this purpose. A visit to our laboratories by Professor Franz Rys of ETN-Lausanne was made as part of this collaboration. An ongoing interaction with Professor T. Takeno of Nagoya University is aimed largely at further investigations of flamelet chemistry.

6. Summary of Inventions

No invention disclosures are to be filed on the basis of work done during the reporting period. The invention disclosure filed during the previous reporting period is still being evaluated by the University's patent counsel.